Kα X-ray emission spectra from highly charged Fe ions in EBIT [1]

V.L. Jacobs and P. Beiersdorfer

Abstract: A detailed spectral model has been developed for the computer simulation of the $2p \rightarrow 1s$ Kα X-ray emission from highly charged Fe ions in the electron beam ion trap (EBIT). The spectral features of interest occur in the range 1.84–1.94 Å. The fundamental radiative emission processes associated with radiationless electron capture or dielectronic recombination, inner-shell electron collisional excitation, and inner-shell-electron collisional ionization are taken in account. For comparison, spectral observations and simulations for high-temperature magnetic-fusion (tokamak) plasmas are reviewed. In these plasmas, small departures from steady-state corona-model charge-state distributions can occur because of ion transport processes, while the assumption of equilibrium (Maxwellian) electron energy distributions is expected to be valid. Our investigations for EBIT have been directed at the identification of spectral features that can serve as diagnostics of extreme nonequilibrium or transient ionization conditions, and allowance has been made for general (non-Maxwellian) electron energy distributions. For the precise interpretation of the high-resolution X-ray observations, which may involve the analysis of blended spectral features composed of many lines, it has been necessary to take into account the multitude of individual fine-structure components of the Kα radiative transitions in the ions from Fe XVIII to Fe XXV. At electron densities higher than the validity range of the corona-model approximation, collisionally induced transitions among low-lying excited states can play an important role. It is found that inner-shell-electron excitation and ionization processes involving the complex intermediate ions from Fe XVIII to Fe XXI produce spectral features, in the wavelength range from 1.89 to 1.94 Å, which are particularly sensitive to density variations and transient ionization conditions.

PACS Nos.: 52.72.+v, 32.80.Dz, 32.70.Fw, 32.30.Rj

Résumé : Nous avons développé un modèle spectral détaillé pour simuler sur ordinateur l'émission-X $2p \rightarrow 1s$ Kα d'ions de fer fortement ionisés dans un piège ionique à faisceau d'électrons (EBIT). Les caractéristiques spectrales qui nous intéressent se trouvent dans le domaine de 1,84 à 1,94 Å. Nous tenons compte des mécanismes fondamentaux d'émission radiative associés à la capture électronique sans radiation ou la recombination diélectrique, l'excitation collisionnelle des électrons des couches internes et l'ionisation des électrons des couches internes. Nous passons en revue pour comparaison les observations spectrales et les simulations pour des plasmas de haute température générés en fusion à confinement magnétique (tokamak). Dans ces plasmas, de petites déviations hors du régime stationnaire des distributions d'état de charge du modèle corona peuvent se produire à cause de mécanismes de transport ionique, alors que l'hypothèse de distribution maxwellienne en énergie est présumée rester valide. Nos études pour EBIT ont eu pour but d'identifier les caractéristiques spectrales qui peuvent servir de diagnostique de situations fortement hors d'équilibre ou d'ionisation transitoire, tout en tenant compte des distributions électroniques générales en énergie (non maxwellienne). Il a été nécessaire de tenir compte de la multitude de composants individuels de structure fine des transitions radiatives Kα des ions allant du Fe XVIII au Fe XXV, afin d'en venir à une interprétation précise des observations de rayons X de haute résolution, qui peuvent impliquer l'analyse de fondus spectraux composés de plusieurs lignes individuelles. Aux densités électroniques plus élevées que le domaine de validité de l'approximation du modèle corona, les transitions induites par collisions parmi les états excités de basse énergie peuvent alors jouer un rôle important. Nous trouvons que les mécanismes d'excitation et d'ionisation des électrons des couches intérieures impliquant les ions intermédiaires complexes du Fe XVIII au Fe XXI produisent des caractéristiques spectrales, dans le domaine des longueurs d'onde de 1,89 ào 1,94 Å, qui sont particulièrement sensibles aux variations de densité et aux conditions d'ionisation transitoire.

[Traduit par la Rédaction]

1. Introduction

Kα emissions associated with $2p \rightarrow 1s$ inner-shell-electron radiative transitions in highly ionized Fe ions occur as prominent satellite line features in the X-ray spectra of laboratory and astrophysical plasmas. We have been developing a detailed atomic physics model [1] for the computer simulation of the Kα emissions produced by the iron ions from Fe XVIII to Fe XXIV, which occur in the spectral range from 1.84 to 1.94 Å. From an analysis of the Kα emission spectra, it is often possible to deduce information concerning the basic physical proper-

Received 2 May 2007. Accepted 5 June 2007. Published on the NRC Research Press Web site at http://cjp.nrc.ca/ on 12 February 2008.

V.L. Jacobs.[2] Center for Computational Materials Science, Code 6390.2, Materials Science and Technology Division, Naval Research Laboratory, Washington, DC 20375-5000, USA.
P. Beiersdorfer. Department of Physics and Advanced Technologies, Lawrence Livermore National Laboratory, P.O. Box 808, Livermore, CA 94550, USA.

[1] Paper given at the Workshop on Twenty Years of Spectroscopy with EBIT held in Berkeley, California, 13–15 November 2006.
[2] Corresponding author (e-mail: Jacobs@dave.nrl.navy.mil).

 doi: 10.1139/P07-104 © 2008 NRC Canada

ties within the emitting region, such as temperatures, densities, and charge-state distributions. In the development of atomic physics models for the computer simulation of the emission spectra due to atomic radiative transitions in plasmas, it has been traditional to assume that the plasma electrons can be adequately represented by a Maxwellian electron velocity (or energy) distribution function. In previous applications [1, 2] of our detailed atomic physics model, computer simulations for low-density (solar corona), intermediate-density (tokamak), and high-density (laser produced) plasmas have been carried out with the assumption that a Maxwellian electron energy distribution provides an adequate representation. In this paper, we review the earlier work and present results obtained from a generalization of our previously reported investigations, in which an arbitrary electron energy distribution can be accommodated.

Elementary transitions involving auto-ionizing resonances of multiply charged ions are known to play important roles in the determination of the atomic-level population densities and charged-state distributions [3]. Radiative transitions from auto-ionizing levels can appear in the emission spectra as prominent satellite features [4] in the vicinity of a resonance line of the ion with one electron removed, for example, the recombining ion in the two-step dielectronic recombination processes described by Burgess [5]. If the initial auto-ionizing state of the ion Fe^{+z}, with residual charge z, is denoted by j and the final bound state is denoted by k, the spontaneous radiative emission process of interest is associated with the single-photon transition,

$$Fe^{+z}(j) \rightarrow Fe^{+z}(k) + \hbar\omega \tag{1}$$

where ω is the photon angular frequency. The spectral features produced by the radiative transitions may appear as distinct spectroscopically resolvable satellite lines, as unresolvable enhancements of the associated resonance line, or as blends of overlapping satellite lines. For the precise computer simulation of the Kα emission spectra, it is necessary to take into account the separate contributions from the individual fine-structure components of the $2p \rightarrow 1s$ inner-shell-electron radiative transitions. Accordingly, the states j and k will be treated as fine-structure states, which are eigenstates of the total electronic angular momentum J (hyperfine structure will be ignored). The auto-ionizing states j of interest may be described as being approximately associated with the electronic configurations $1s^1 2s^r 2p^s$ (with $0 \leq r \leq 2$ and $0 \leq s \leq 6$) in the irons ions from Fe XVIII to Fe XXIV. However, it is understood that these identifications cannot have a rigorous meaning within the framework of a fully relativistic multiconfiguration representation for the many-electron atomic states.

In high-temperature plasmas, the auto-ionizing states denoted by j can be populated by the radiationless electron-capture process

$$Fe^{+(z+1)}(i) + e^-(\varepsilon_i) \rightarrow Fe^{+z}(j) \tag{2}$$

which is the first step in the two-step dielectronic recombination process that usually provides the dominant recombination mechanism at low densities [5]. These auto-ionizing states can decay by the inverse auto-ionization process or alternatively by means of the stabilizing radiative transition described by (1). In low-density plasmas, the initial ions undergoing radiationless electron capture can be assumed to be predominantly in their ground states. However, the dominant auto-ionization process may correspond to a transition leading to the formation of an excited state i of the residual ion [6]. This results in a reduction of the branching ratio for the stabilizing radiative transition, which is the second step in the two-step dielectronic recombination process. In addition, auto-ionization into excited states following radiationless electron capture can provide an important indirect (resonant) contribution to the total cross section or rate of electron impact excitation [7].

While radiationless electron capture is often the dominant excitation mechanism for the Kα emission in a high-temperature plasma, which is then commonly referred to as dielectronic-recombination satellite emission, it is also necessary to take into account the population of the auto-ionizing states as a result of the inner-shell-electron electron-impact excitation process,

$$Fe^{+z}(i') + e^-(\varepsilon_{i'}) \rightarrow Fe^{+z}(j) + e^-(\varepsilon_j) \tag{3}$$

In addition, auto-ionization (instead of radiative decay) following inner-shell-electron excitation provides an important indirect (resonant) contribution to the total cross section or rate for electron impact ionization [8].

In the development of our earlier atomic physics model [1] for the computer simulation of the Kα radiative emission of highly charged Fe ions, account was taken of only radiationless electron capture and inner-shell-electron collisional excitation due to electron impact. In subsequent investigations [9, 10], our atomic physics model has been extended to take into account the additional population of the auto-ionizing states that is produced by the inner-shell-electron electron-impact ionization process,

$$Fe^{+(z-1)}(i'') + e^-(\varepsilon_{i''}) \rightarrow Fe^{+z}(j) + e^-(\varepsilon_j) + e^-(\varepsilon'_j) \tag{4}$$

While the radiationless electron capture process is expected to play the dominant role in plasmas under conditions near a steady-state ionization–recombination balance, for example, as described by the low-density corona-model approximation discussed by Griem [11], inner-shell-electron collisional excitation and ionization processes can provide the dominant Kα line-formation mechanism during nonequilibrium transient-ionzation situations.

In the development of atomic physics models for the computer simulation of the Kα emission spectra, it has usually been assumed that the electron velocity distribution can be adequately represented by a local-thermodynamic-equilibrium (Maxwellian) distribution function. The radiative emission spectra can then be predicted as functions of the local electron temperature. In this paper, we describe an extension of our formulation of the theory of the atomic radiative transitions following electron–ion collisions in which account can be taken of an arbitrary single-electron velocity (or energy) distribution function. To investigate the radiative emission spectra produced by extreme nonequilibrium electron energy distributions, we have carried out computer simulations for the Fe Kα emission spectra obtained from the electron beam ion trap (EBIT) facility [12, 13] at the Lawrence Livermore National Laboratory. Since the electron beam in EBIT is nearly mono-energetic, a precise investigation of the various fundamental Kα radiative emission processes can be carried out. To observe the contributions from the dielectronic recombination satellites, which are produced by radiationless electron capture, it has been necessary to set the electron-beam energy at a particular resonance position [14] or to vary the electron-beam energy in a continuous

© 2008 NRC Canada

manner through the resonance region [15]. We discuss the observed and theoretically predicted Fe Kα radiative emission spectra for two different nonresonant electron-beam energies, which occur above and below the K-shell ionization threshold. At these nonresonant electron-beam energies, the dielectronic recombination process cannot contribute to the total radiative emission. From the comparison between the observed high-resolution Fe Kα radiative emission spectra and the corresponding theoretically predicted spectra, the contributions from inner-shell-electron collisional excitation and ionization have been separately investigated, and their sensitivity to density variations and transient ionization conditions has been individually accessed [9].

The decomposition of the Kα radiative emission spectra into the separate contributions associated with the three fundamental electron–ion collision processes cannot be made in an unambiguous manner and is strictly applicable only for low densities, for which the simple corona-model approximation can be assumed to be valid. In our investigation of the effects of increasing electron density on the various Kα radiative-emission features, which are mainly attributed to electron collisional transitions among the low-lying fine-structure states of the radiating ion, it should be emphasized that a complete picture of the density variations of the radiative emission spectra can only be provided on the basis of a detailed (possibly time-dependent) collisional-radiative model, in which the populations of both the bound and auto-ionizing states of the atomic ions are determined by taking into account the multitude of elementary (state-specific) collisional and radiative transitions. To provide an approximate description of the density dependence of the Kα radiative-emission spectra, we have introduced a hierarchy of simple statistical models [1] for the distribution of the population of the initial ions among the various low-lying fine-structure states. The additional collisional transitions among the auto-ionizing states, which can lead to strong density variations in dense laser-produced plasmas [16–18], have not been taken into account in our present Kα spectral simulations. The simple statistical models have been introduced to provide a convenient treatment for the multitude of the fine-structure components that must be taken into account.

The remainder of this paper has been organized in the following manner. In Sect. 2, we present a brief discussion of the theoretical foundation for the determination of the spectral intensity of the Kα radiative-emission processes. We give particular emphasis to the convenient, but approximate decomposition of the total spectral intensity into the contributions associated with the three fundamental electron–ion collisional interactions. Allowing for an arbitrary single-electron energy distribution, expressions are presented for the parameters (rate coefficients) describing these three collisional interactions. In Sect. 3, we describe the determination of the charge-state distributions of the radiating atomic ions. While the charge-state distributions in low-density high-temperature equilibrium plasmas are determined predominately by the (possibly dynamical) balance between electron-impact ionization (including auto-ionization following inner-shell-electron excitation) and direct radiative together with dielectronic recombination, a different physical situation is usually encountered in the description of the charge-state balance in extreme nonequilibrium or transient-ionization plasmas. In Sect. 4, we present the results of our Kα spectral observations and theoretical predictions for both equilibrium and nonequilibrium conditions. We emphasize the different roles that the various fundamental atomic processes can be expected to play under these different conditions. Particular emphasis has been given to the identification of spectral features that are sensitive to density variations and transient-ionization conditions. Finally, our conclusions are presented in Sect. 5, in which brief discussions are presented on the need in a future extension of this investigation for a more sophisticated atomic kinetics calculation [3], incorporating a detailed determination of the fine-structure level populations and a more complete quantum-mechanical description [19], taking into account the angular distribution and polarization of the emitted photons. This will be required for the precise investigation of the radiation observed during directed-electron collisional excitation processes [20].

2. Spectral intensity due to Kα radiative emission

At sufficiently low densities, the total spectral intensity of the Kα radiative emission may be expressed as a sum of contributions associated with the individual (two-step) line-formation mechanisms. In this investigation, account has been taken of the radiative emission following radiationless electron capture (dielectronic recombination), inner-shell-electron collisional excitation, and inner-shell-electron collisional ionization. The total spectral intensity produced by the various arrays of fine-structure radiative transitions $j \rightarrow k$ in all abundant Fe ions (with residual charge z) can be expressed in the form:

$$I(\hbar\omega) = \sum_z \sum_j \sum_k B_r(z, j \rightarrow k) L(z, j \rightarrow k, \hbar\omega) \times \Big[C_{\mathrm{cap}}(z+1, i, \varepsilon_i \rightarrow j) N(z+1) N_e + C_{\mathrm{exc}}(z, i', \varepsilon_{i'} \rightarrow j) N(z) N_e + C_{\mathrm{ion}}(z-1, i'', \varepsilon_{i''} \rightarrow j) N(z-1) N_e \Big] \quad (5)$$

In this expression, which may be considered as representing a generalization of our previously developed Kα spectral model [1] to include ionization, the isolated-resonance approximation has been adopted and the quantum-mechanical interference effects [21, 22] between resonant and nonresonant transitions have been neglected.

The population densities of the initial ions in the three adjacent stages of ionization are denoted by $N(z+1)$, $N(z)$, and $N(z-1)$, and the electron density is denoted by N_e. The initial states of these ions are denoted by i, i', and i'', respectively. The rate coefficients denoted by C_{cap}, C_{exc}, and C_{ion} describe the population of the auto-ionizing states j from the initial states in the radiationless electron capture, inner-shell-electron collisional excitation, and inner-shell-electron collisional ionization processes, respectively. In a general description of the two-step initial-state population kinetics, which could be based on a steady-state or time-dependent collisional-radiative model, summations should be performed over the initial states in the three adjacent stages of ionization. In the present investigation, either the initial ions are assumed to be in the ground fine-structure state or a hierarchy of statistical population models [1] is adopted, in which the summations over initial fine-structure

© 2008 NRC Canada

substates are approximately represented by the introduction of average rate parameters and total charge-state populations.

To provide a precise description of the high-resolution Kα radiative emission spectra, it is necessary to treat the auto-ionizing states j and the final bound states k in the radiative transitions $j \rightarrow k$ as individual fine-structure states, which are specified in terms of the total electronic angular-momentum quantum numbers J_j and J_k, respectively (hyperfine structure has been ignored in our investigation). In our low-density corona-model description [1], in which all excited states are assumed to undergo decay only by either spontaneous radiative transitions or auto-ionization processes, the total spectral intensity can be expressed in terms of the familiar radiative branching ratios $B_r(z, j \rightarrow k)$, which are given by:

$$B_r(z, j \rightarrow k) = \frac{A_r(z, j \rightarrow k)}{\sum_i A_{\text{auto}}(z, j \rightarrow i, \varepsilon_i) + \sum_{k'} A_r(z, j \rightarrow k')} \quad (6)$$

The denominator of this expression represents the total decay rate that is obtained as the sum of the individual auto-ionization rates $A_{\text{auto}}(z, j \rightarrow i, \varepsilon_i)$, together with the sum of the individual spontaneous radiative decay rates $A_r(z, j \rightarrow k)$. The angular-frequency-normalized spectral lineshape functions, which are denoted by $L(z, j \rightarrow k, \hbar\omega)$, are assumed to be determined (in the low-density regime) predominantly by Doppler broadening and the broadening due to the permissible auto-ionization and spontaneous radiative decay processes. In the Livermore EBIT facility, the radiating ions may be described as quasi-stationary, i.e., as undergoing negligible movements during the effective radiative lifetime. Consequently, the role of the Doppler effect is expected to be diminished substantially.

In the binary-collision approximation that has been employed in our simple low-density spectral emission model [1], the overall atomic excitation process has been described as involving the separate (uncorrelated) actions of the three fundamental electron–ion collisional interaction processes consisting of radiationless electron capture, inner-shell-electron collisional excitation, and inner-shell-electron collisional ionization. Assuming that the interactions with the plasma electrons can be adequately represented in terms of a single-electron velocity distribution function $f_\varepsilon(\boldsymbol{v}_\varepsilon)$ [23], the rate coefficients C_{cap}, C_{exc}, and C_{ion} for the three fundamental electron–ion collisional interaction processes may be related to the corresponding differential electron–ion collision cross sections σ_{cap}, σ_{exc}, and σ_{ion} in the following manner [24]:

$$C_{\text{cap}}(z+1, i, \varepsilon_i \rightarrow j) = \iint \mathrm{d}\boldsymbol{v}_e \mathrm{d}\Omega |\boldsymbol{v}_e| f_e(\boldsymbol{v}_e) \sigma_{\text{cap}}(z+1, i, \varepsilon_i \rightarrow j; \boldsymbol{v}_e, \Omega) \quad (7)$$

$$C_{\text{exc}}(z, i', \varepsilon_{i'} \rightarrow j) = \iint \mathrm{d}\boldsymbol{v}_e \mathrm{d}\Omega |\boldsymbol{v}_e| f_e(\boldsymbol{v}_e) \sigma_{\text{exc}}(z, i', \varepsilon_{i'} \rightarrow j; \boldsymbol{v}_e, \Omega) \quad (8)$$

$$C_{\text{ion}}(z-1, i'', \varepsilon_{i''} \rightarrow j) = \iint \mathrm{d}\boldsymbol{v}_e \mathrm{d}\Omega |\boldsymbol{v}_e| f_e(\boldsymbol{v}_e) \sigma_{\text{ion}}(z-1, i'', \varepsilon_{i''} \rightarrow j; \boldsymbol{v}_e, \Omega) \quad (9)$$

In these relationships, averages have been performed over the initial electron velocities $\boldsymbol{v}_\varepsilon$ and integrations have been carried out over the angles Ω, referring to the final scattered electrons. (Integration over the energy and angles of the ejected electron are also assumed to have been carried out in the definition of the electron-impact ionization cross section σ_{ion}.) If many-body correlation effects become important, as in a strongly coupled plasma, it may be necessary to adopt a more fundamental many-body kinetic-theory description [25–28], in which the concept of a binary-collision cross section is no longer well defined.

The cross section $\sigma_{\text{cap}}(z+1, i, \varepsilon_i \rightarrow j)$ describing the radiationless electron capture process can be simply related to the decay rate $A_{\text{auto}}(z, j \rightarrow i, \varepsilon_i)$ for the inverse auto-ionization process, and relativistic multiconfiguration atomic structure calculations, using the code developed by Cowan [29], have been carried out [1] to provide accurate values for the auto-ionization and radiative transition rates. While sophisticated methods have been developed for the determination of the cross sections describing the electron–ion collisional excitation and ionization processes, such as those based on the distorted-wave and close-coupling approaches, we have adopted relatively simple approximations [1] to provide estimates for the multitude of fine-structure transitions that must be taken into account in the computer simulation of the Kα radiative emission spectra. For the electron-impact excitation cross section denoted by $\sigma_{\text{exc}}(z, i', \varepsilon_{i'} \rightarrow j)$, we have employed the Born and Bethe (long-range dipole) approximations [30], which provide a convenient expression [1] in terms of the atomic statistical weights, the excitation energy, and the radiative transition rate (or Einstein A coefficient) $A_r(z, j \rightarrow i')$ describing the spontaneous (electric-dipole) radiative decay process.

The final contribution to the spectral intensity involves the electron-impact ionization cross section $\sigma_{\text{ion}}(z-1, i'', \varepsilon_{i''} \rightarrow j)$, corresponding to the excitation of the residual ion to the fine-structure state j. To obtain the cross section of interest, it is necessary to carry out an average over the initial fine-structure magnetic substates corresponding to $MJ_{i''}$ and a summation over the final fine-structure magnetic substates corresponding to MJ_j. In addition, the desired cross section, which is defined in terms of integrations over the energy and angles of the ejected electron, involves summations over the total angular-momentum quantum numbers representing the combined ejected-electron residual-ion system. For example, in the Born approximation and in the LS-coupling representation the cross section can be expressed in terms of summations over the allowed values of the angular momenta L, S, and J for the combined system. If a central-field picture is adopted for the description of the many-electron atomic states, one obtains the surprisingly simple result that the ionization cross section connecting the specific fine-structure states i'' and j is reducible to the cross section for the ionization of an electron from the active initial subshell $n_{i''}\ell_{i''}$. To take into account the presence of more than one initial $n_{i''}\ell_{i''}$ electron, a factor of $N_{i''}$ should be included. For the precise treatment of complex electronic structures, it may be necessary to include the appropriate coefficient of fractional parentage. In the application to the Kα spectral analysis, we have adopted the simple procedure of using the semi-empirical ionization cross sections obtained by Lotz [31] for ionization from the 1s shell, including a factor of "2" to take into account the number of initial bound K-shell electrons. Finally, it should be pointed out that for incident electron energies sufficient to

© 2008 NRC Canada

produce inner-shell-electron ionization, it may be necessary to consider additional line-formation mechanisms, such as cascade transitions from higher lying excited states.

In the prediction of the Kα radiative emission spectra from laboratory and astrophysical plasmas, it has been customary to make the assumption that equilibrium conditions have been established within the subsystem consisting of the plasma electrons. Accordingly, the electron velocity (energy) distribution function $f_\varepsilon(\boldsymbol{v}_\varepsilon)$ has been taken to be a Maxwellian corresponding to an electron temperature T_e. In the Livermore EBIT facility, extreme nonequilibrium conditions have been achieved. The appropriate electron velocity distribution function $\mathrm{f}_\varepsilon(\boldsymbol{v}_\varepsilon)$ then represents a nearly mono-energetic distribution, with an energy spread of only about 50 eV [14, 15]. Consequently, the radiative emission spectra are expected to be more sensitive to the detailed energy variations of the individual electron–ion collision cross sections and to the associated energy-conservation restrictions. In particular, the radiationless electron capture process, which is the first-step in the dielectronic recombination process that often plays the dominant role in the formation of the Kα spectra in high-temperature plasmas, can occur in electron–ion beam interactions only for resonant (or nearly-resonant) values of the incident electron-beam energy. While the dielectronic satellite spectra have been observed with high-resolution in EBIT experiments [14] in which the incident electron energy was varied either in a step-wise or in a continuous manner through the resonant region, the present work focuses on EBIT measurements performed for nonresonant values of the incident electron energy, which were either below or above the K-shell ionization threshold of Fe XXIV (8.7 keV). Consequently, the radiationless electron capture process does not play any role in the formation of the Kα radiative emission spectra observed under these conditions, and the observed spectra can be described taking into account the remaining two processes of inner-shell-electron collisional excitation and ionization.

For a precise prediction of the radiative emission spectra, it is clearly necessary to provide a detailed evaluation of the spectral line-shape functions $L(z, j \rightarrow k, \hbar\omega)$. For the computer simulation of the Kα radiative emission spectra observed in the present EBIT experiment, where the detailed spectral line shapes of the individual fine-structure components have not been resolved, only the accurate knowledge of the spectral line positions has been required. However, the accurate prediction of the Kα spectral line positions has presented a more difficult problem than might have been anticipated, because of the inadequacies of the relativistic multiconfiguration atomic structure calculations. For the calculation of the spectral line positions, we have adopted the simple correction procedure described by Seely et al. [32]. In this procedure, the Kα spectral line positions corresponding to a given Fe ion are uniformly adjusted by a wavelength correction, which is taken to be between 0.002 and 0.003 Å. However, in comparisons between the theoretical predictions and the observed spectra, we found that it was necessary to employ experimentally determined line positions for various Kα transitions [2]. Without doing so, it is not possible to reproduce the shape of the observed spectrum in regions of substantial line blending, i.e., in the wavelength region above 1.89 Å. To provide a fundamental treatment for the spectral line positions that would result in a precise agreement with the observed high-resolution Fe Kα emission spectra, it will be necessary to take into account the quantum electrodynamical radiative corrections to the individual many-electron atomic energy levels. In lowest order perturbation theory, these radiative corrections can be obtained as the sums of the electron self-energies and the vacuum-polarization energies, as discussed by Mohr [33].

3. Charge-state distributions

At sufficiently low densities, where the atomic ions can be assumed to be predominantly in their ground electronic states, the concept of a charge-state distribution is meaningful. Ignoring charge-exchange processes, the dynamical balance between the electron–ion ionization and recombination processes can be described by the following set of partial differential equations for the number densities $N(z)$ in the various charge states:

$$\frac{\partial N(z)}{\partial t} + \nabla \bullet [\boldsymbol{V}(z)\, N(z)] = N_\mathrm{e} N(z-1) S(z-1 \rightarrow z) - N_\mathrm{e} N(z) S(z \rightarrow z+1) + N_\mathrm{e} N(z+1) \alpha(z+1 \rightarrow z) - N_\mathrm{e} N(z) \alpha(z \rightarrow z-1) \quad (10)$$

The ionization and recombination rate coefficients S and α occurring on the right-hand side of this set of equations correspond to effective transition rates, which are most rigorously introduced as a result of a reduced kinetic-theory description [3, 34] of the atomic collisional and radiative interactions. When time-dependent phenomena and transport processes, which are described by the terms occurring on the left-hand side, are neglected, this set of equations can be reduced to the familiar steady-state corona-model relationships governing the charge-state distributions in a low-density plasma,

$$N(z) S(z \rightarrow z+1) = N(z+1) \alpha(z+1 \rightarrow z) \quad (11)$$

Within the low-density corona-model approximation, the effective ionization and recombination rates are given, in the isolated-resonance approximation and with the neglect of the quantum-mechanical interference between the resonant and nonresonant transition amplitudes, by the familiar expressions as sums of the direct (nonresonant) and the indirect (resonant) contributions. The total ionization rate coefficient S can be expressed as the sum of the rate coefficients S_ion for direct (nonresonant) electron-impact ionization and the contributions for indirect (two-step) ionization due to auto-ionization following inner-shell-electron collisional excitation [34],

$$S_\mathrm{ion}(z \rightarrow z+1) = \sum_j \Big[S_\mathrm{di}(g \rightarrow j) + \sum_a C_\mathrm{ex}(g \rightarrow a) Q^{-1}(a,a) A_\mathrm{a}(a \rightarrow j) \Big] \quad (12)$$

In the corona-model approximation, the collisional-radiative transition matrix $\mathbf{Q}$ has only diagonal elements $Q(a, a)$. These diagonal elements, which correspond to the inverse of the total lifetimes, are given as the sums of the auto-ionization and spontaneous radiative decay rates, as expressed by the denominator of (6). The indirect contribution to the overall ionization rate can provide a significant enhancement for ions with a relatively large number of inner-shell electrons. Additional indirect mechanisms, such as double auto-ionization following radiationless

© 2008 NRC Canada

Fig. 1. Corona-model charge-state distributions $N(z)/N_T$ as functions of the electron temperature T_e, predicted for highly charged Fe ions in equilibrium plasmas.

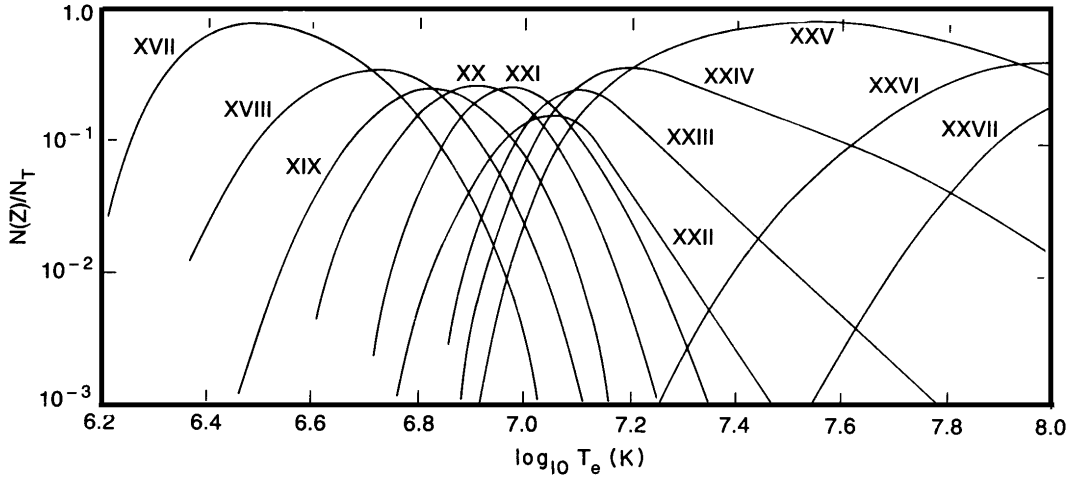

electron capture, have been investigated and have been found to be important in special cases. For sufficiently deep inner-shell-electron vacancies in heavy atoms, the cascade decay process involving a sequence of radiative, Auger, and Coster-Kronig transitions can result in a state of multiple ionization [35].

The total recombination rate coefficient a can be expressed as the sum of the direct (nonresonant) radiative recombination rate coefficients α_{rr} and the indirect (two-step) dielectronic recombination rate coefficients [34],

$$\alpha(z+1 \rightarrow z) = \sum_b \Big[\alpha_{rr}(i \rightarrow b) + \sum_a C_{cap}(i \rightarrow a) Q^{-1}(a,a) A_r(a \rightarrow b)\Big] \quad (13)$$

It should be pointed out that the class of auto-ionizing resonances that contributes to the indirect (two-step) dielectronic recombination rate is usually distinct from the class of auto-ionizing states that provides the indirect (two-step) ionization rate due to auto-ionization following inner-shell-electron collisional excitation. Moreover, the dominant contributions to the dielectronic recombination rates of low- and medium-Z atomic ions are usually associated with auto-ionizing resonances corresponding to highly excited states of the outer (recombining) electron. Even in the low-density corona-model approximation, the precise evaluation of the dielectronic recombination rates represents an immensely difficult endeavor for complex ions [36, 37], for example, M-shell ions.

For low-density equilibrium plasmas, in which the electron velocity distribution can be adequately represented by a Maxwellian equilibrium distribution function corresponding to an electron temperature T_e, the overall ionization and recombination rate coefficients S_{ion} and α_{rec} can be evaluated as functions of the electron temperature. At higher densities, for which the important excited and auto-ionizing states can be appreciably depopulated by collisional transitions, a reduced kinetic-theory description can be developed [34] in which the ground-state (and possibly a few low-lying metastable excited-state) population densities satisfy a set of partial differential equations of the same form as the set given by (10). To obtain useful expressions for the reduced effective ionization and recombination rate coefficients, which are now functions of the electron density N_e and the electron temperature T_e, it has been necessary to invoke the assumption that the excited and auto-ionizing states that are not explicitly included can be represented by their steady-state population densities. In the numerical evaluation of the expressions obtained for the reduced effective transition rates, it has been necessary to assume that the local-thermodynamic-equilibrium (Boltzmann–Saha) relationships provide adequate approximations for the population densities of the very highly excited bound and auto-ionizing levels. Calculations have been carried out [34] that lead to the prediction that the reduced effective recombination rate coefficients can be strong functions of the electron density N_e.

The total corona-model electron–ion ionization and recombination rate coefficients S and α have been evaluated as functions of the temperature T_e for a representative selection of elements [6], including those that are abundant in astrophysical plasmas and those that have been of interest in both magnetic confinement and laser fusion research. Using these total electron–ion ionization and recombination rate coefficients, the corona-model charge-state distributions have been determined [6] as functions of the electron temperature. The results that have been obtained for highly charged Fe ions are presented in Fig. 1. The total electron–ion ionization and recombination rate coefficients can also be employed for the determination of the charge-state distributions taking into account transport processes and time variations, which are known to produce small or moderate departures from the corona-model charge-state distributions in tokamak plasmas [38]. In our computer simulations of the high-resolution Kα radiative-emission spectra obtained from tokamak plasmas [2], the multi ion species transport code MIST [39], developed at the Princeton Plasma Physics Laboratory, has been employed. It should be emphasized that these total electron–ion ionization and recombination rate coefficients have been evaluated with the assumption that a Maxwellian equilibrium velocity distribution has been established for the subsystem consisting of the plasma electrons.

Equilibrium charge-state distributions have been measured for highly charged Fe ions in EBIT [40] as functions of electron beam energy. The results are shown in Fig. 2. A comparison is presented with the theoretical predictions, which take into

© 2008 NRC Canada

Fig. 2. Charge-state distributions determined from X-ray observations and theoretically predicted from a model calculation. The triangles, diamonds, squares, and circles refer to Fe^{26+}, Fe^{25+}, Fe^{24+}, and Fe^{23+}, respectively. The continuous-line curves represent the results of the theoretical predictions with an assumed oxygen background density of 1.05×10^7 cm^{-3}. (The charge-state distribution for Fe^{22+} is not shown; it is less than 0.01.) The statistical error bars are of the order of the size of the points.

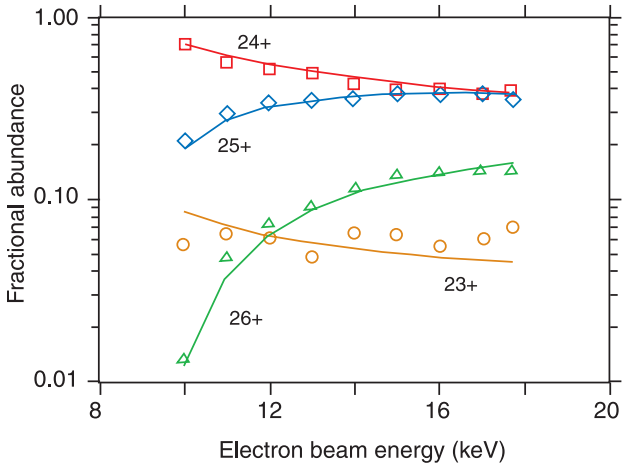

account direct ionization and direct radiative recombination. These predictions also allow for charge exchange recombination. To achieve the good agreement between the measurements and the theoretical predictions seen in Fig. 2, it was necessary to include charge exchange from an oxygen background gas with a density as high as 1.05×10^7 cm^{-3}. Accordingly, charge exchange recombination was found to be dominant over direct radiative recombination in these EBIT plasmas. Differences between the measurements and the theoretical predictions are apparent for the lithium-like fraction. This can be attributed to the measurement uncertainty. The Fe charge-state distribution has been measured in numerous other investigations on the Livermore EBIT facility, although generally no comparison with model calculations has been made. In Fig. 3, we show the charge-state distribution that has been derived from an L-shell Fe spectrum measured at an electron-beam energy of 2.93 keV [41]. This charge-state distribution was derived from a fit of direct collisional-excitation lines with the theoretical cross sections, adjusted to reflect the individual line ratios that were measured in a crystal spectrometer.

Some extreme transient-ionization conditions have also been achieved and recorded at the Livermore EBIT facility [9, 10, 42, 43]. These extreme conditions resemble those that can occur in certain nonequilibrium laboratory and astrophysical plasmas, for example, supernova remnants. Using a semi-empirical procedure [9, 43], the time-dependent charge-state distributions have been theoretically predicted, taking into account direct ionization, direct radiative recombination, and charge exchange. This procedure is similar to that employed to calculate the equilibrium distributions presented in Fig. 2. The nonequilibrium charge-state distributions predicted for highly charged Fe ions in EBIT are shown in Fig. 4 for an electron-beam energy of 12 keV, which is above the K-shell ionization threshold. These calculations were used to successfully model the observed spectra [9, 10]. Some examples will be given in the next section.

Fig. 3. Charge-state distribution derived for the spectrum taken at 2.93 keV. This charge-state distribution was derived from a fit of direct collisional-excitation lines with the theoretical cross sections, adjusted to reflect the individual line ratios that were measured in the crystal spectrometer.

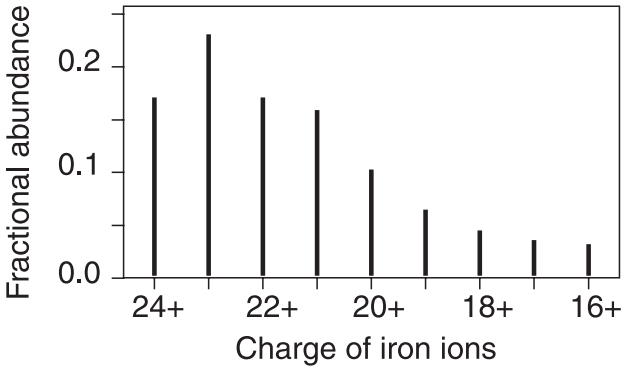

Fig. 4. Nonequilibrium charge-state distributions (relative abundances) as functions of time, predicted for highly charged Fe ions in the electron beam ion trap (EBIT) for an electron-beam energy of 12 keV.

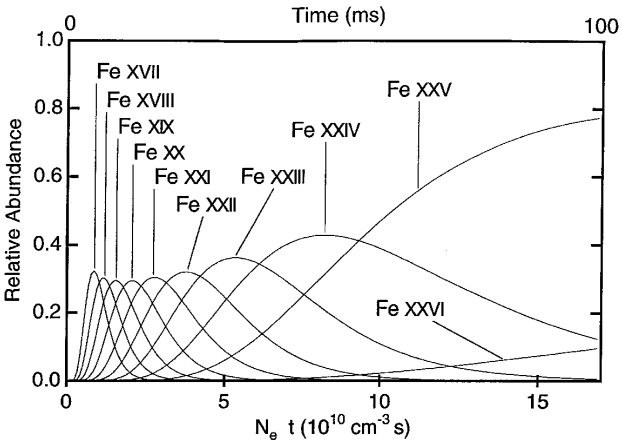

It should be emphasized that a more comprehensive and detailed model is expected to be required for the precise determination of the charge-state distributions that are responsible for the Kα radiative emission during electron–ion beam interactions. Although the simple charge balance model used to predict the Fe charge-state distributions both in equilibrium and transient EBIT plasmas shown in Figs. 2 and 4, respectively, was very successful, this success was achieved as a result of adjusting the contribution from charge exchange recombination by varying the assumed neutral gas pressure to best fit the measurements. This procedure may not correctly reflect the individual contributions of the ionization and recombination rates, and it cannot be further validated because the neutral gas pressure in the trap is not known independently. Accordingly, this procedure provides an indication of the accuracy with which ionization and radiative rates should be determined. Fully ab initio calculations would require a much more comprehensive and detailed knowledge of the individual rates. In fact, a so-called "all-ion" model, in which the excitation and ionization processes are treated as coupled for all eight charge states of oxygen, was needed to reproduce the Kα emission of oxygen

© 2008 NRC Canada

observed in extreme transient-ionzation conditions at the Livermore EBIT facility [44]. Analogous calculations may be needed if very high precision is required in predicting the Fe charge distribution in an ab initio manner.

4. Spectral simulations for Kα emission

At very low electron densities ($N_e \leq 10^{10}$ cm^{-3}), for which the simple corona-model approximation is expected to be valid, the three fundamental electron–ion collisional processes, consisting of radiationless electron capture, inner-shell-electron collisional excitation, and inner-shell-electron collisional ionization, can be assumed to occur predominantly from atomic ions that are initially in their ground fine-structure states. In addition, all excited states can be assumed to undergo de-excitation only by auto-ionization or by spontaneous radiative emission processes. Fe Kα radiative-emission spectra from low-density plasmas have been theoretically predicted [1] as functions of the electron temperature T_e in accordance with a well-defined procedure, which is based on the simple form of the low-density corona-model formulation. The spectral intensities thereby obtained show a dependence on the electron density N_e in accordance with the simple N_e^2 law that is characteristically associated with binary-collision encounters in quasi-neutral plasmas.

For intermediate charge states of Fe ions (Fe XVIII–Fe XXI) in a tokamak plasma or in the Livermore EBIT facility, where the electron density N_e usually occurs in the intermediate-density regime $10^{12} \leq N_e \leq 10^{14}$ cm^{-3}, collisional transitions among the initial fine-structure states of the ground-state electronic configuration can produce a more complicated density dependence of the Kα spectral intensities. The precise treatment of this density dependence would involve the implementation of a detailed (possibly time-dependent) collisional-radiative model, in which account would be taken of all important elementary collisional and radiative transitions in the determination of the population densities for the multitude of the relevant atomic fine-structure states. To provide an approximate description of the density dependence of the Kα radiative emission spectra, we have introduced [1] a hierarchy of simple statistical population models to represent the distribution of the initial atomic ions among the relevant fine-structure states. This hierarchy of simple statistical population models has also been adopted by Shlyaptseva et al. [45]. This simple statistical description leads to a modification of the low-density corona-model formulation in which account is taken of the approximate statistical-equilibrium relationship:

$$\frac{N(z,i)}{N(z)} \approx \frac{g(z,i)}{\sum_{i'} g(z,i')} g(z,i) = 2J_i + 1 \qquad (14)$$

An approximate description, which is believed to be appropriate for the intermediate-density regime $10^{12} \leq N_e \leq 10^{14}$ cm^{-3}, can be provided by assuming that the elementary collisional transitions are capable of establishing a statistical-equilibrium distribution of the initial ion population among only the fine-structure states belonging to the ground-state electronic configuration. Accordingly, the summation over i' in (14) is restricted to include only the initial fine-structure states associated with the ground-state electronic configuration. For an approximate description of the atomic-population kinetics in high-density (laser produced) plasmas, where the electron density can be produced within the high-density regime $10^{20} \leq N_e \leq 10^{24}$ cm^{-3}, the summation over i' in (14) may be extended to include the initial fine-structure states associated with the electronic configurations that can be derived from the ground-state electronic configuration by means of a $2s \rightarrow 2p$ excitation. At very high (laser-produced plasma) densities, for which $N_e > 10^{24}$ cm^{-3}, the elementary collisional transitions connecting the auto-ionizing states can play an important role. The spectral intensity of the radiative emission from the auto-ionizing states can then become a strong function of the electron density [16, 17]. This density sensitivity has become recognized as an important characteristic of dense plasmas [18], which may provide a useful indication of the attainment of the desired high-density compression in laser-fusion experiments.[3]

Our previously reported computer simulations [1, 2] of the Fe Kα radiative emission spectra have been carried out for high-temperature plasmas under near-equilibrium conditions, including solar-flare plasmas, tokamak plasmas, and laser produced plasmas. In these high-temperature plasmas, the Kα radiative emissions were assumed to be produced predominantly as a result of radiationless electron capture (dielectronic recombination) and inner-shell-electron collisional excitation. The charge-state distributions, which are required in the evaluation of the spectral intensities, have been determined from the steady-state balance between direct ionization, together with auto-ionization following inner-shell-electron collisional excitation, and direct radiative combined with dielectronic recombination. In tokamak plasmas, small or moderate departures from the corona-model charge-state distributions can be produced by the effects of impurity-ion transport processes [39]. In these spectral simulations, the plasma electrons were assumed to be adequately represented by a single-electron equilibrium (Maxwellian) velocity distribution function. In our computer simulations of the high-resolution Fe Kα radiative-emission spectra observed on the Livermore EBIT facility, the Kα spectra lines, which have been observed for nonresonant incident electron-beam energies, have been assumed to be formed only by inner-shell-electron collisional excitation and ionization processes. By selecting one of the two incident electron-beam energies to occur below the K-shell ionization threshold, the contributions from the collisional excitation processes can be investigated separately. The two selected incident electron-beam energies fall outside the regions of the auto-ionizing resonances. Accordingly, the radiationless electron capture process does not play any role in the present EBIT experiment. In the semi-empirical description of the charge-state distributions, which has been employed in the analysis of the X-ray spectra from EBIT [9,10,43], account has been taken of direct electron-impact ionization, direct radiative recombination, and charge-exchange. The Kα spectral simulations for EBIT may be considered as providing a microscopic investigation of the effects of extreme nonequilibrium electron velocity distributions and transient ionzation conditions. In Table 1, we present a summary of the atomic processes that play dominant roles in the determination of the Kα radiative-emission spectra and the charge-state distributions, contrasting the cases of near-equilibrium (tokamak) plasmas and transient-ionization (EBIT) conditions.

We have presented [1, 2] a complete description of the mul-

[3] H.R. Griem, R.C. Elton, and B.L. Welch. Private communication. 1998.

© 2008 NRC Canada

Table 1. Dominant processes in the determination of the Kα radiative emissions and the charge-state distributions in near-equilibrium plasmas and under transient-ionzation conditions.

Plasma conditions	Near equilibrium (for example, Tokamak plasmas)	Transient ionization (for example, electron beam ion trap (EBIT)
Dominant Kα line excitation processes	Radiationless electron capture (dielectronic recombination)	Radiationless electron capture (only for resonant beam energies)
	Inner-shell electron excitation	Inner-shell electron excitation
		Inner-shell electron ionization
Processes determining the charge-state distributions	Direct ionization auto-ionization following inner-shell-electron excitation	Direct ionization auto-ionization following inner-shell-electron excitation
	Radiative recombination dielectronic recombination	Radiative recombination
	Ion transport	Charge exchange

Table 2. Selected $2p \rightarrow 1s$ Fe Kα spectral line identifications, indicating sensitivity to density variations. This list of lines consists of fine-structure transitions from boron-like (denoted by B), carbon-like (denoted by C), nitrogen-like (denoted by N), and oxygen-like (denoted by O) Fe ions.

Label	Ion	Transition	Wavelength (Å)[a]
B3	Fe XXII	$^2P_{3/2} \rightarrow ^2P_{3/2}$	1.8817
B4	Fe XXII	$^2P_{1/2} \rightarrow ^2P_{1/2}$	1.8826
C6	Fe XXI	$^1D_2 \rightarrow ^3P_2$	1.8933
C8	Fe XXI	$^3P_2 \rightarrow ^1D_2$	1.8945
C9	Fe XXI	$^3D_1 \rightarrow ^3P_0$	1.8945
N5	Fe XXI	$^2P_{3/2} \rightarrow ^4S_{3/2}$	1.90520
N6	Fe XX	$^2D_{5/2} \rightarrow ^2D_{5/2}$	1.90565
N7	Fe XX	$^2D_{3/2} \rightarrow ^2D_{3/2}$	1.90605
N11	Fe XX	$^4P_{5/2} \rightarrow ^4S_{3/2}$	1.90845
O3	Fe XIX	$^1P_1 \rightarrow ^1D_2$	1.91625
O4	Fe XIX	$^3P_2 \rightarrow ^3P_2$	1.91700

[a]Measured or semi-empirical fit from Beiersdorfer et al. [2].

titude of the $2p \rightarrow 1s$ fine-structure radiative transitions that have been taken into account in our computer simulations of the Fe Kα radiative-emission spectra from high-temperature plasmas. In our EBIT investigations, we have placed particular emphasis on the identification of spectral line features that are sensitive to variations in the electron density or to extreme nonequilibrium conditions corresponding to transient ionization. In Table 2, we present a summary of the prominent spectral line features that are most sensitive to density variations. This list of lines consists of transitions from boron-like (denoted by B), carbon-like (denoted by C), nitrogen-like (denoted by N), and oxygen-like (denoted by O) Fe ions. These four charge states of Fe have a ground-state electronic configuration that consists of multiple fine-structure levels, which are readily populated in the intermediate density regime, and these charge states can therefore produce a complicated density dependence of the Kα spectral intensities. For example, the fine-structure levels of the ground-state electronic configuration of carbon-like Fe are, in increasing energy:

(1) $1s^2_{1/2}2s^2_{1/2}2p^2_{1/2}\,^3P_0$

(2) $1s^2_{1/2}2s^2_{1/2}2p_{1/2}2p_{3/2}\,^3P_1$

Table 3. Selected $2p \rightarrow 1s$ Fe Kα spectral line identifications, indicating sensitivity to transient-ionization conditions. This list consists of transition z from helium-like Fe, transitions o and p from lithium-like Fe, transition E16 from beryllium-like Fe, and several transitions from boron-like, nitrogen-like, oxygen-like, and fluorine-like Fe ions.

Label	Ion	Transition	Wavelength (Å)[a]
z	Fe XXV	$^3S_1 \rightarrow ^1S_0$	1.8681
o	Fe XXIV	$^2S_{1/2} \rightarrow ^2P_{3/2}$	1.8968
p	Fe XXIV	$^2S_{1/2} \rightarrow ^2P_{1/2}$	1.8922
E16	Fe XXIII	$^3P_1 \rightarrow ^3S_0$	1.8793
B10	Fe XXII	$^4P_{1/2} \rightarrow ^2P_{1/2}$	1.8922
N7	Fe XX	$^2D_{3/2} \rightarrow ^2D_{3/2}$	1.90605
O5	Fe XIX	$^3P_1 \rightarrow ^3P_0$	1.91825
F1	Fe XVIII	$^2S_{1/2} \rightarrow ^2P_{3/2}$	1.9264
F2	Fe XVIII	$^2S_{1/2} \rightarrow ^2P_{1/2}$	1.9305

[a]Measured or semi-empirical fit from Beiersdorfer et al. [2].

(3) $1s^2_{1/2}2s^2_{1/2}2p_{1/2}2p_{3/2}\,^3P_2$

(4) $1s^2_{1/2}2s^2_{1/2}2p^2_{3/2}\,^1D_2$

(5) $1s^2_{1/2}2s^2_{1/2}2p^2_{3/2}\,^1S_0$

As the density increases, the ground fine-structure state (1) is no longer the only fine-structure state that is populated. Therefore, electron-impact collisions may now produce K-shell excitations in carbon-like Fe ions that are in states (2) through (5), resulting in clearly different lines than from K-shell excitations involving carbon-like Fe ions in state (1). For example, the K-shell excitation of state (1) will readily populate the $1s_{1/2}2s^2_{1/2}2p^2_{1/2}2p^3_{3/2}D_1$ upper level. This level will then radiatively decay back down to the ground fine-structure state (1), producing the line C9 indicated in Table 2. As the density increases, the population in state (1) diminishes and line C9 becomes weaker. At the same time, line C6 becomes stronger. This line is produced via K-shell excitation from level (3) to the $1s_{1/2}2s^2_{1/2}2p_{1/2}2p^2_{3/2}\,^1D_2$ upper level and subsequently decays back down to level (3).

In Table 3, we present a summary of the prominent spectral line features that are most sensitive to transient-ionzation

© 2008 NRC Canada

conditions. This list consists of transition z from helium-like Fe, transitions o and p from lithium-like Fe, transition E16 from beryllium-like Fe, and several transitions from boron-like, nitrogen-like, oxygen-like, and flourine-like Fe ions. These lines have in common that they can be produced by inner-shell ionization of the ground level of the neighboring charge state. For example, line z is produced by K-shell ionization of the $1s^2 2s$ ground state of lithium-like Fe, accompanied by the population of the $1s2s\ ^3S_1$ upper level of line z. Similarly, lines o and p are produced by K-shell ionization of the $1s^2 2s^2$ ground state of beryllium-like Fe, together with the population of the $1s2s^2\ \ ^2S_{1/2}$ upper level common to both lines; line E16 is produced by ionization of the $1s^2 2s^2 2p_{1/2}$ ground state of boron-like Fe, with the population of the $1s2s^2 2p_{1/2}\ \ ^3P_1$ upper level.

Using the statistical-population model that is believed to be appropriate for the description of the intermediate-density plasma region corresponding to $10^{12} \leq N_e \leq 10^{14}$ cm^{-3}, in which the initial-ion population is assumed to be statistically distributed among the fine-structure states associated with the ground-state electronic configuration, computer simulations have been performed for the Kα spectral intensities [1]. The results that have been obtained for near-equilibrium (Tokamak) plasmas are presented in Fig. 5 for an electron temperature of $T_e = 1.0 \times 10^7$ K. In this figure, the observed Kα spectra from the PLT Tokamak [2] is compared with the computer simulations for both the low-density and intermediate-density populations models that we have introduced. In these spectral simulations, account has been taken of radiationless electron capture (dielectronic recombination) and inner-shell-electron collisional excitation. Radiationless electron capture has been found to provide the dominant contributions, but a few prominent spectral lines have been identified for which the only nonvanishing contributions correspond to inner-shell-electron collisional excitation. The synthesized Kα radiative-emission spectrum for the intermediate-density population models has been found to be in good agreement with the high-resolution X-ray spectra obtained from the PLT Tokamak [2]. Even better agreement with the experimental data has been obtained [2] by using the spectral intensity coefficients that are associated with the individual charge states as input to a computer simulation based on the multi-ion-species transport software program MIST [39], in which account is taken of the departures from corona-model charge-state distributions that are the result of the effects of radial ion-transport processes. These transport processes connect plasma regions with different values of the electron temperature and density. Although these Kα spectral simulations have been performed assuming the validity of an equilibrium (Maxwellian) single-electron velocity distribution, it is widely believed that appreciable non-Maxwellian components (which are often referred to as high-energy tails) of the electron velocity distribution can be produced during the augmentation of the usual Ohmic heating mechanism by intense microwave absorption processes.

Spectra obtained during extreme nonequilibrium from EBIT [9] are shown in Fig. 6. Here we show the K-shell spectra of iron in the region 1.84–1.94 Å excited by an electron-beam energy of 12 keV. Five spectra are shown, each of which was recorded for a duration of 20 ms after the injection of iron into the electron beam ion trap. As a result, the time-dependent evolution of the spectra driven by changes in the ionization balance is clearly seen. Because the beam energy is well above the energy required

Fig. 5. (*a*) Fe Kα spectral intensity observed on the PLT Tokamak compared with theoretical predictions based on (*b*) the intermediate-density, and (*c*) the low-density population models described in the text. The electron temperature was $T_e = 1.0 \times 10^7$ K. In the atomic physics model used for the theoretical predictions, account has been taken of radiationless electron capture (dielectronic recombination) and inner-shell-electron collisional excitation.

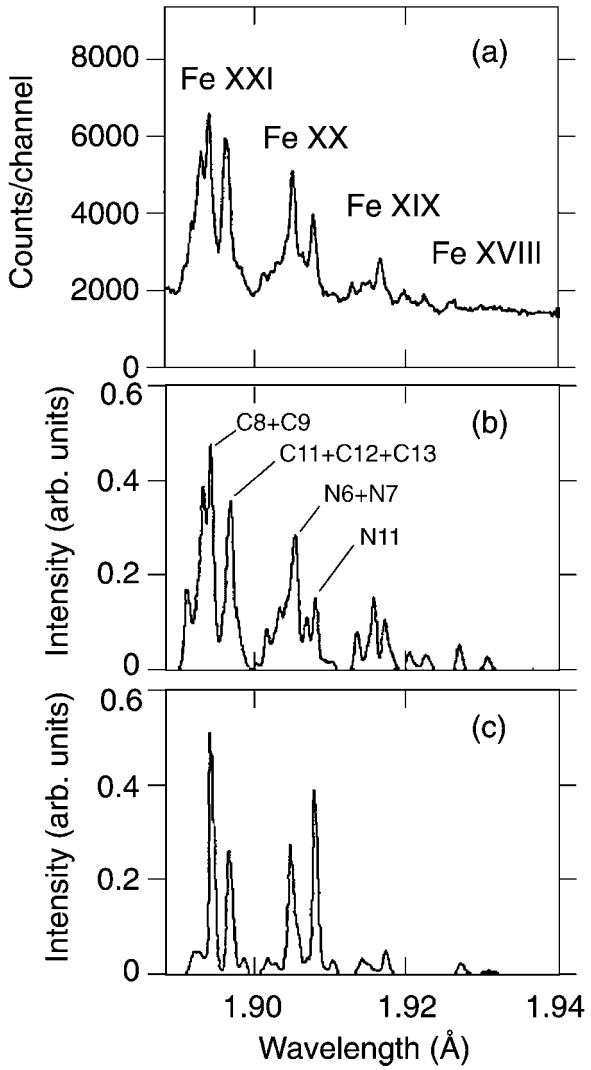

for K-shell ionization, the signature of line formation by inner-shell ionization is readily observed. The Fe K-shell lines listed in Table 3 can be seen to be greatly enhanced over their intensity in the absence of inner-shell ionization. Line z in Fe XXV, for example, is seen to be more intense than the Fe XXV resonance line w in these ionizing plasmas.

In Fig. 7, we present our Fe Kα spectral simulations for the transient-ionzation conditions that have been achieved in the Livermore EBIT facility for an incident electron-beam energy of 12 keV [10]. The individual spectral contributions due to the collisional excitation and collisional ionization mechanisms are separately presented for the ions Fe XVIII–Fe XXI in the low-density and intermediate-density population regimes introduced in connection with the atomic population model. For comparison, we also present the Fe K-shell spectra observed

© 2008 NRC Canada

Fig. 6. K-shell spectra of iron in the region 1.84–1.94 Å, measured at the Livermore EBIT facility at an electron-beam energy of 12 keV. The spectra were observed under transient-ionization conditions. The observations are the first five spectra, each of which was recorded for a duration of 20 ms after the injection of iron into the electron beam ion trap.

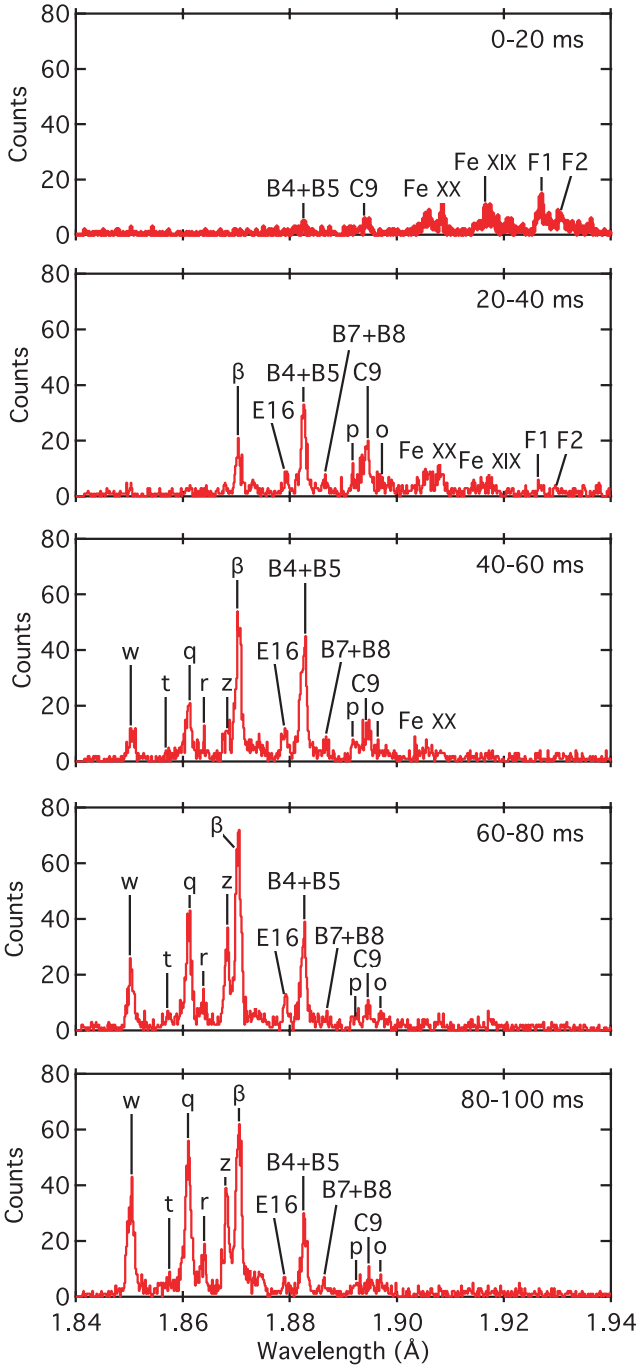

in the region 1.885–1.940 Å. Since the incident electron-beam energy has been selected to occur outside the region of the auto-ionizing resonances, the radiationlesss electron capture (dielectronic recombination) process does not play any role in the determination of the Kα spectral intensities (for comparison, see Fig. 8). Accordingly, the observed high-resolution X-ray spectra are formed by inner-shell-electron collisional ex-

Fig. 7. Kα radiative-emission spectra from Fe XVIII–Fe XXI in the wavelength range 1.89–1.94 Å. The theoretically predicted spectral results are given for the contributions from collisional excitation in (*a*) the low-density regimes and (*b*) intermediate-density regimes and and from K-shell ionization in the (*c*) low-density and (*d*) intermediate density regimes. The spectral-line-intensity coefficients have been been calculated assuming equal populations for the four charge states contributing to these spectra. The observed K-shell spectra of iron in the region 1.885–1.94 Å (*e*) have been measured on the EBIT-II electron beam ion trap under transient-ionzation conditions at a beam energy of 12 keV. The experimental results were obtained during the first 7 ms after the injection of iron into the trap.

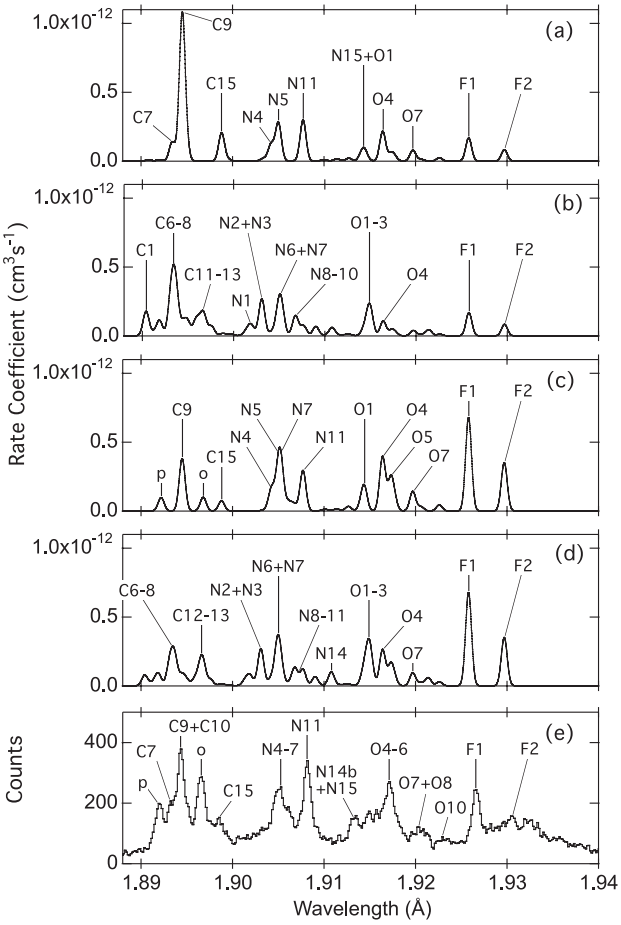

citation and ionization. The spectral simulations show spectral features (from Tables 2 and 3) involving the complex intermediate ions from Fe XVIII to Fe XXI, which are found to be particularly sensitive to density variations and transient-ionzation conditions.

The simple low-density corona-model approximation has been found to be inadequate for the accurate simulation of the observed spectra from EBIT. As seen from Fig. 7, some characteristics, such as the size of C9, can only explained by the assumption of a higher density. However, the intermediate-density approximation, which has provided an adequate description for the Tokamak observations, appears to overestimate the ground-state fine-structure mixing. A finer density grid may be needed for the accurate simulation of the EBIT spectra.

Decaux et al. [10] presented detailed level populations in Fe XXI, as illustrated in Fig. 9. This figure shows the relative

© 2008 NRC Canada

Fig. 8. The spectra of K-shell emission lines for helium-like, lithium-like, and beryllium-like Fe ions for four different electron-beam energies: (*a*) 4.55 keV, (*b*) 4.61 keV, (*c*) 4.68 keV, and (*d*) 4.76 keV. The spread in beam energies is about 50 eV. As a result, the first three energies occur within the region of the dielectronic-recombination resonances, and the observed lines are therefore produced by the dielectronic recombination. The fourth energy is above the threshold for electronic-impact excitation of the helium-like states and outside of the resonance region. The observed lines are thus excited by electron collisions.

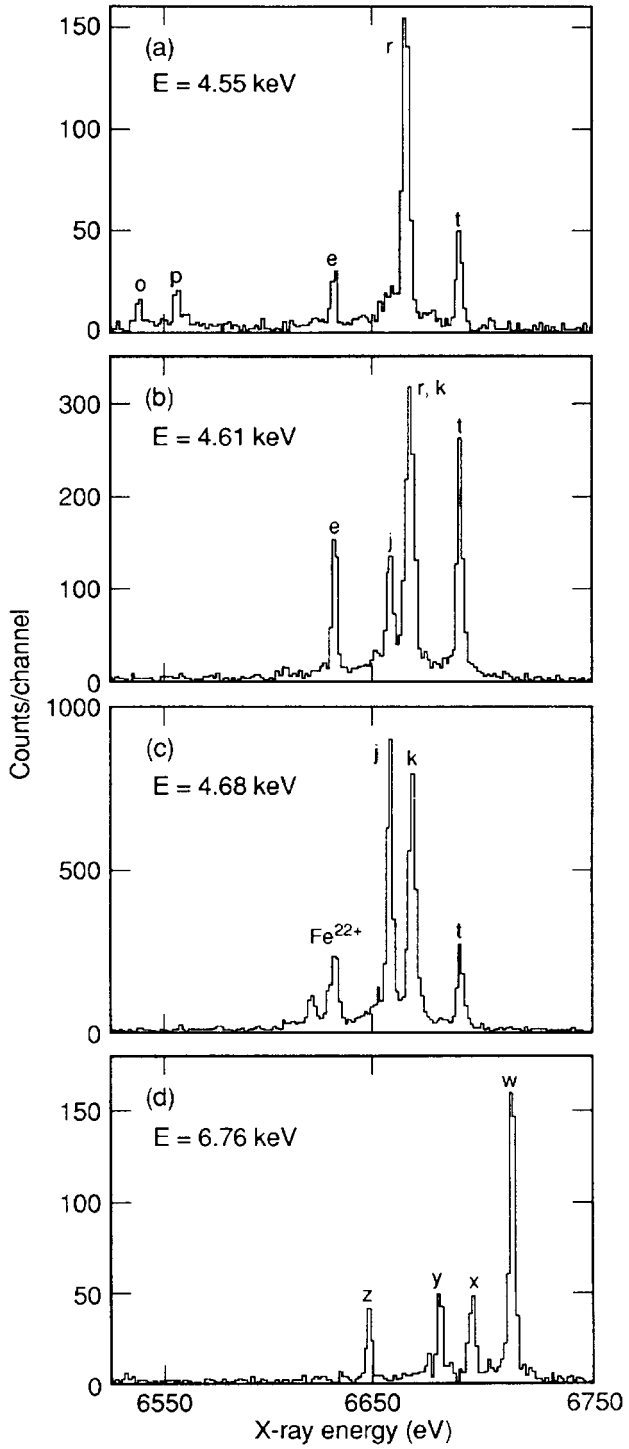

Fig. 9. Relative populations of the first four ground-state configuration fine-structure levels as functions of the electron density for Fe XXI. The electron-energy distribution has been taken to be a Maxwellian equilibrium distribution corresponding to an electron temperature, centered at 1.6 keV.

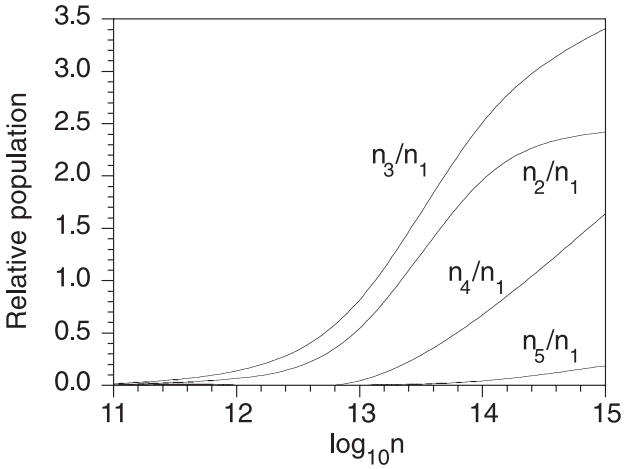

populations of the individual excited fine-structure levels of the ground-state electronic configurations as functions of electron density (within the range from 10^{11} to 10^{15} cm^{23}). These level populations have been determined from a collisional-radiative-model calculation using the Hebrew University Lawrence Livermore Laboratory Atomic Code (HULLAC) [46], with collisional rate coefficients computed assuming Maxwellian electron energy distributions. Since the experimental results from the EBIT-II electron-beam ion trap at Livermore were obtained using a highly nonequilibrium electron-energy distribution, which was not taken into account in these calculations, the results in Fig. 9 should be understood to provide only a qualitative representation of the relative populations pertaining to the electron-beam measurements. Fe XXI together with Fe XIX are the only two charge states for which electron–ion collisionally induced mixing of the ground-state-configuration fine-structure states is found to be significant at electron densities equal to or less than 10^{12} cm^{23}, i.e., for the density regime typically found in EBIT plasmas.

The results presented in Fig. 9 indicate that the ground electronic configuration fine-structure states have relative populations that are continuous functions of the electron density. Because the collisional redistribution of the population among the ground-state fine-structure levels has been found to have important consequences in the determination of the spectral line intensities for several of the ions of interest at the densities pertaining to the spectral observations, this serves to emphasize the importance of a refined, collisional-radiative model treatment of the electron-density-dependent collisional redistribution of the atomic-level populations.

5. Conclusions

In plasmas with near equilibrium conditions, the Kα radiative-emission spectra are produced predominantly by the processes of radiationless electron capture (dielectronic recombination) and inner-shell-electron collisional excitation. In the EBIT facility at the Lawrence Livermore National Laboratory, radi-

© 2008 NRC Canada

ationless electron capture can occur only for resonant incident electron-beam energies, and the high-resolution Kα radiative emission observed in the present experiment is produced by inner-shell-electron collisional excitation and inner-shell-electron collisional ionization. Moreover, inner-shell-electron collisional excitation and ionization processes in EBIT, involving the complex intermediate ions from Fe XVIII to Fe XXI, give rise to Kα spectral features that are particularly sensitive to density variations. In addition, the signature of K-shell inner-shell ionization, which reflects to transient-ionization conditions, can be seen in selected lines of Fe XVIII through Fe XXV. It can be expected that similar spectral-line formation conditions will prevail in extreme nonequilibrium transient-ionization plasmas with non-Maxwellian electron velocity (or energy) distributions.

For a fundamental treatment of the density dependence of the Kα radiative spectral emission, it will be necessary to develop in a future extension of this investigation a detailed time-dependent collisional-radiative model description of the dynamical, fine-structure-resolved excitation and ionization processes, taking into account all important elementary atomic collisional and radiative transitions. Using a density-matrix approach [47], a self-consistent treatment can be provided for the atomic-population kinetics and the spectral-line shapes. For a precise description of the Kα spectral emission produced by directed-electron interactions, it will be necessary to incorporate into the simulation program a treatment of the angular distribution and polarization of the emitted photons [19].

Acknowledgments

This research work has been supported by the US Department of Energy (DOE) and by the Office of Naval Research. Work at LLNL was performed under the auspices of the DOE under contract No. W-7405-Eng-48 and supported by the National Aeronautics and Space Administration's Astronomy and Physics Research and Analysis Program under grant NNG06WF08I.

References

1. V.L. Jacobs, G.A. Doschek, J.F. Seely, and R.D. Cowan, Phys. Rev. A, **39**, 2411 (1989).
2. P. Beiersdorfer, T. Phillips, V.L. Jacobs, K.W. Hill, M. Bitter, S. von Goeler, and S.M. Kahn. Ap. J. **409**, 846 (1993).
3. V.L. Jacobs. J. Quant. Spectrosc. Radiat. Transfer, **54**, 195 (1995).
4. C.P. Bhalla, A.H. Gabriel, and L.P. Presnyakov. Mon. Not. R. Astron. Soc. **172**, 359 (1975).
5. A. Burgess. Astrophys. J. **139**, 776 (1964).
6. V.L. Jacobs. Astrophys. J. **296**, 121 (1985).
7. V.L. Jacobs, P.L. Hagelstein, M. Chen, R.K. Jung, and J.F. Seely. Phys. Rev. A, **41**, 1041 (1990).
8. L. Goldberg, A.K. Dupree, and J.W. Allen. Ann. Astrophys. **28**, 589 (1965).
9. V. Decaux, P. Beiersdorfer, S.M. Kahn, and V.L. Jacobs. Ap. J. **482**, 1076 (1997).
10. V. Decaux, V.L. Jacobs, P. Beiersdorfer, D.A. Liedahl, and S.M. Kahn. Phys. Rev. A, **68**, 012509 (2003).
11. H.R. Griem. Plasma spectroscopy. McGraw-Hill, New York. 1964.
12. M.A. Levine, R.E. Marrs, J.R. Henderson, D.A. Knapp, and M.B. Schneider. Phys. Scr. T. **22**, 157 (1988).
13. M.A. Levine, R.E. Marrs, J.N. Bardsley, P. Beiersdorfer, C.L. Bennett, M.H. Chen, T. Cowan, D. Dietrich, J.R. Henderson, D.A. Knapp, A. Osterheld, B.M. Penetrante, M.B. Schneider, and J.H. Scofield. Nucl. Instrum. Methods Phys. Res. Sect. B, **43**, 431 (1989).
14. P. Beiersdorfer, T.W. Phillips, K.L. Wong, R.E. Marrs, and D.A. Vogel. Phys. Rev. A, **46**, 3812 (1992).
15. D.A. Knapp, P. Beiersdorfer, M.H. Chen, J.H. Scofiled, and D. Schneider. Phys. Rev. Lett. **74**, 54 (1995).
16. A.V. Vinogradov, I.Yu. Skobelev, and E.A. Yukov. Sov. Phys. JETP, **45**, 925 (1977).
17. V.L. Jacobs and M. Blaha. Phys. Rev. A, **21**, 525 (1980).
18. A. Zigler, V.L. Jacobs, D.A. Newmam, P.G. Burkhalter, D.J. Nagel, T.S. Luk, A. Mc Pherson, K. Boyer, and C.K. Rhodes. Phys. Rev. A, **45**, 1569 (1992).
19. V.L. Jacobs and A.B. Filuk. Phys. Rev. A, **60**, 1975 (1999).
20. P. Beiersdorfer, D.A. Vogel, K.J. Reed, V. Decaux, J.H. Scofield, K. Widmann, G. Hölzer, E. Förster, O. Wehrhan, D.W. Savin, and L. Schweikhard. Phys. Rev. A, **53**, 3974 (1996).
21. S.L. Haan and V.L. Jacobs. Phys. Rev. A, **40**, 80 (1989).
22. V.L. Jacobs, J. Cooper, and S.L. Haan. Phys. Rev. A, **36**, 1093 (1987).
23. N.A. Krall and A.W. Trivelpiece. Principles of plasma physics. McGraw-Hill, New York. 1973.
24. J. Oxenius. Kinetic theory of particles and photons. Springer-Verlag, Berlin, Germany. 1986.
25. D.C. Montgomery and D.A. Tidman. Plasma kinetic theory. McGraw-Hill, New York. 1964.
26. N. Rostoker, R. Aamodt, and O. Eldridge. Ann. Phys. **31**, 243 (1965).
27. D.F. DuBois. *In* Lectures in theoretical physics. Vol. IX C, *Edited by* W.E. Brittin. Gordon and Breach, Science Publishers, Inc., New York. 1967.
28. N.N. Bogoliubov and K.P. Gurov. ZETP, **17**, 614 (1947).
29. R.D. Cowan. Theory of atomic structure and spectra. University of California Press, Berkeley, California. 1981.
30. H.A. Bethe. Ann. Phys. (Leipzig) **5**, 325 (1930).
31. W. Lotz. Astrophys. J. Suppl. **14**, 207 (1967).
32. J.F. Seely, U. Feldman, and U.I. Safronova. Astrophys. J. **304**, 838 (1985).
33. P.J. Mohr. Phys. Rev. A, **32**, 1949 (1985).
34. V.L. Jacobs and J. Davis. Phys. Rev. A, **18**, 697 (1978).
35. V.L. Jacobs and B.F. Rozsnyai. Phys. Rev. A, **34**, 216 (1986).
36. M.H. Chen. Phys. Rev. A, **47**, 4775 (1993).
37. E. Behar, P. Mendelbaum, J.L. Schwob, A. Bar-Shalom, J. Oreg, and W.H. Goldstein. Phys. Rev. A, **54**, 3070 (1996).
38. M. Bitter, S. von Goeler, N. Sauthoff, K. Hill, K. Brau, D. Eames, M. Goldman, E. Silver, and W. Stodiek. *In* International conference on X-ray processes and inner-shell ionization, Stirling, Scotland, 1980, *Edited by* D.J. Fabian, H. Kleinpoppen, and L.M. Watson. Plenum Press, New York. 1981. p. 861.
39. R.A. Hulse. Nucl. Technol. Fusion, **3**, 259 (1983).
40. K.L. Wong, P. Beiersdorfer, R.E. Marrs, B.M. Penetrante, K.J. Reed, J.H. Scofield, D.A. Vogel and R. Zasadzinski. Nucl. Instrum. Methods Phys. Res. Sect. B, **72**, 234 (1992).
41. H. Chen, M.F. Gu, P. Beiersdorfer, K.R. Boyce, G.V. Brown, S.M. Kahn, R.L. Kelley, C.A. Kilbourne, F.S. Porter, and J.H. Scofield. Ap. J. **646**, 653, (2006).
42. V. Decaux and P. Beiersdorfer. Phys. Scr. T, **47**, 80 (1993).
43. V. Decaux, P. Beiersdorfer, A. Osterheld, M. Chen, and S.M. Kahn. Astrophys. J. **443**, 464 (1995).

© 2008 NRC Canada

44. M.-F. Gu, M. Schmidt, P. Beiersdorfer, H. Chen, D.B. Thorn, E. Träbert, E. Behar, and S.M. Kahn. Astrophys. J. **627**, 1066 (2005).
45. A.S. Shlyaptseva, I.E. Golovkin, and U.I. Safronova. J. Quant. Spectrosc. Radiat. Transfer, **56**, 157 (1996).
46. A. Bar-Shalom, M. Klapisch, and J. Oreg. Phys. Rev. A, **38**, 1773 (1988).
47. V.L. Jacobs, J. Cooper, and S.L. Haan. Phys. Rev. A, **50**, 3005 (1994).

© 2008 NRC Canada